Investigation of fine activated carbon as a viable flow electrode in capacitive deionization

Gbenro Folaranmi, Myriam Tauk, Mikhael Bechelany, Philippe Sistat, Marc Cretin, Francois Zaviska

Investigation of fine activated carbon as a viable flow electrode in capacitive deionization.

Gbenro Folaranmi[¥], Myriam Tauk[¥], Mikhael Bechelany *, Philippe Sistat, Marc Cretin and Francois Zaviska*

Institut Européen des Membranes, IEM, UMR-5635, University of Montpellier, ENSCM, CNRS, Place Eugène Bataillon, CEDEX 5, 34095 Montpellier, France; gbenro.folaranmi@etu.umontpellier.fr (G.F.); philippe.sistat@umontpellier.fr (P.S.); marc.cretin@umontpellier.fr (M.C.); francois.zaviska@umontpellier.fr (F.Z.)

* Correspondance : mikhael.bechelany@umontpellier.fr (M.B.), francois.zaviska@umontpellier.fr (F.Z.)

¥ Cofirst authors

Highlights

- Fine particle activated carbon obtained at 90 min dry ball milling exhibits highest salt removal rate
- Ball milling of commercial activated carbon leads to generation of finer particles
- The finer the particles, the lesser the aggregation level
- Increased level of surface contact is created by higher particle numbers
- The smaller the particles, the higher the viscosity and zeta potential

Abstract

Flow capacitive deionization is a variant of capacitive deionization allowing continuous/semi continuous desalination. Performance of electrode is linked to factors such as applied voltage, feed electrode hydrophilicity, carbon loading, conductivity of the feed electrolyte, particle size, viscosity etc. In this paper, a new approach was adopted in reducing the particle size of the carbon used as flow electrode by dry milling method at different time intervals. The particle size and hydrodynamic diameter of the ground activated carbon (fine activated carbon FAC) was reduced after milling in comparison with pristine activated carbon (PAC) but an increase in viscosity was observed in FAC. Increase in viscosity stems from increase in particles loosening which correlates to more stability of the slurry due to higher zeta potential with consequent less particles agglomeration effect and greater force of repulsion.

Physico-chemical analysis such as scanning electron microscopy (SEM) and particle size analyzer confirmed the reduction in size of the particles. On verification as flow electrode at 10 wt. % (carbon loading), fine activated carbon exhibited a significant increase in desalination over pristine activated carbon. The improvement is linked to lower particles aggregation that enables higher ions migration

and contact to the carbon pores; thus this simple method shows that fine activated carbon can be a viable flow electrode in FCDI.

Keywords: Flow electrode capacitive deionization, fine AC, viscosity and desalination.

Graphical abstract

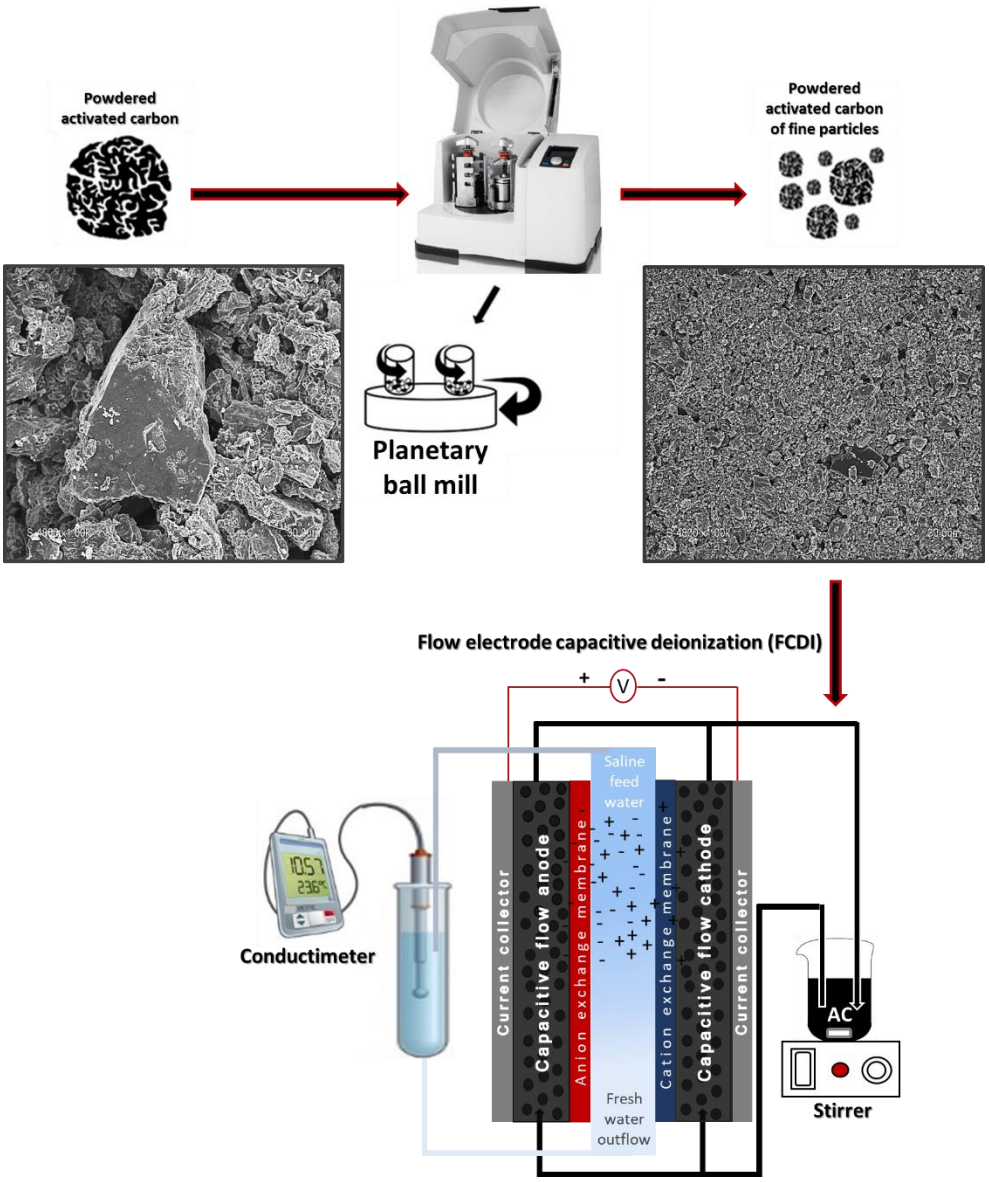

1. Introduction

Flow capacitive deionization (FCDI), a variant of capacitive deionization (CDI) is a novel form of water desalination technology that operates by adsorption method through polarized flow/slurry carbon as flow electrode [1, 2]. It offers both semi-continuous or continuous form of desalination and no limitation of available pores for adsorption; a tremendous advantage over both membrane capacitive deionization (MCDI) and capacitive deionization (CDI) [3].

FCDI, just like (M)CDI operates by ions adsorption due to electric field that is generated when a difference of potential (ΔV = 0.8-1.2 V) is applied from external source to the cell thus creating electrostatic attraction of ions into polarized electrodes. Here, the electrode (carbon slurry) is in flowing state; passing on flow channels (current collector) [4].

Carbon slurry is used as electrode material in FCDI because of its large surface area, porosity, low cost, relative high capacitance and ease of manufacturing from readily available biomass [5, 6]. High carbon loading in FCDI favors good connectivity network among carbon particles (favoring electron transport) but this tremendously leads to high viscosity of the slurry hence clogging is observed inside the flowing channel [4].

As found in literature, reports in FCDI using spherical or hollow carbons of regular shape and size (commercial or tailored made carbons from polymeric precursors) have shown higher desalination performance because they can afford higher carbon loading and relatively low viscosity due to its small surface area to volume ratio. [7, 8]. Recent approaches in improving FCDI desalination performance by optimizing different parameters such as cell potential, cell architecture through fluidized beds to improve carbon loading and additives utilization to mitigate internal electrode resistance of carbon slurry have been reported in literature [9-11]. Aranzazu *et al.* [12], using activated carbon (average diameter of 10 μm) slurry at different weight suspensions to understand the performance of different slurries in relation to their electrochemical behavior. Using commercially made activated carbon (average diameter of 5.6 μm) of indefinite shape and size, Kuo *et al.*, [13] made carbon slurries of different mass loadings (5, 10 and 15 wt. %) and tested their mobility (static, semi flow and flow modes) in relation to desalination performance and energy consumption.

However, studies in verifying the importance of activated carbon particle size to further progress FCDI applications and its consequent effect on electrochemical and rheological properties of AC should be investigated. As known, FCDI performance indices can be easily influenced by various factors such as operating condition, nature of materials etc., thus understanding the correlation of carbon based particle size to FCDI performance and working parameters under non Faradaic condition call for extensive investigation.

To reveal and understand the relationship and condition of operation between the aforementioned above and system performance, the design of activated carbon flow electrodes based on fine particles was explored for the first time in this paper. Hence, this research provides insights into the fundamental understanding of fine activated carbon flow electrodes in comparison to normal activated carbon as flow electrodes in relation to rheology and desalination performances.

Fine activated carbon (FAC) is a modified form of powdered activated carbon (PAC) that is generated by simple crushing or grinding of powdered activated carbon (PAC) into smaller particle size [14]. FAC has found application in water treatment as it has been reported to provide faster adsorption rate and better adsorption capacity for naturally occurring organic matter and metals [15, 16]. However, application of FAC as flow electrode portends a significant increase in viscosity due to their high stability hence striking a compromise between cell carbon loading and desalination performances.

2. Materials and methods.

2.1. Materials

Activated carbon, Darco (CAS no: 7440-44-0) that was chosen for this work because the focal point of our research group with regards to FCDI is to advance and maximize the properties of cheap activated carbon for industrial upscale, and sodium chloride (NaCl, CAS no: 7647-14-5, MW 58.44 g mol^{-1}, 99%) were both purchased from Sigma Aldrich. Cationic and anionic exchange membranes were purchased from Membranes International Inc. (Ringwood, New Jersey, USA) and Deionized water was gotten from (18 MΩ cm^{-2}) purification system.

2.2. FAC Preparation

Few grams of PAC were ball milled (ball mill diameter 50 mm) at a rotation of 350 rpm for 30, 60, 90 min and 5 h respectively at ambient temperature. The ball-milled AC (FAC) is then used as slurry electrode.

2.3. Experimental Procedure

Flow electrode was prepared by weighing an appropriate amount of FAC and then mixed with 1 g/L NaCl solution as electrolyte according to the formulation given in **Table *1***. The mixture was sonicated for about 1 h and then stirred for about 2 h before being fed into the cell. The slurry electrode contained in a beaker was continuously stirred on a magnetic stirrer during the course of the experiment. The schematic diagram of the short circuited close cycle (SCC) experimental configuration is shown in **Erreur ! Source du renvoi introuvable.** in which the cell was powered by a potentiostat and the feed solution (FS, 5 g/L) was made to pass through a spacer sandwiched in between cation and anion exchange membranes. The feed electrodes stored in a reservoir (FE, carbon slurry) were made to pass (by pumping) through flow channels and as they exit the channels, they are fed back to the reservoir and then re-circulated. During this process, the conductivity of the FS was monitored by an ion conductivity meter.

Table 1: Flow Electrode composition

Electrode material	FE (10 wt. %) (g)	[NaCl] (g/L) (70 mL)	FS (g/L) [NaCl]
AC	7.80	1.0	5.0
Fine AC	7.80	1.0	5.0

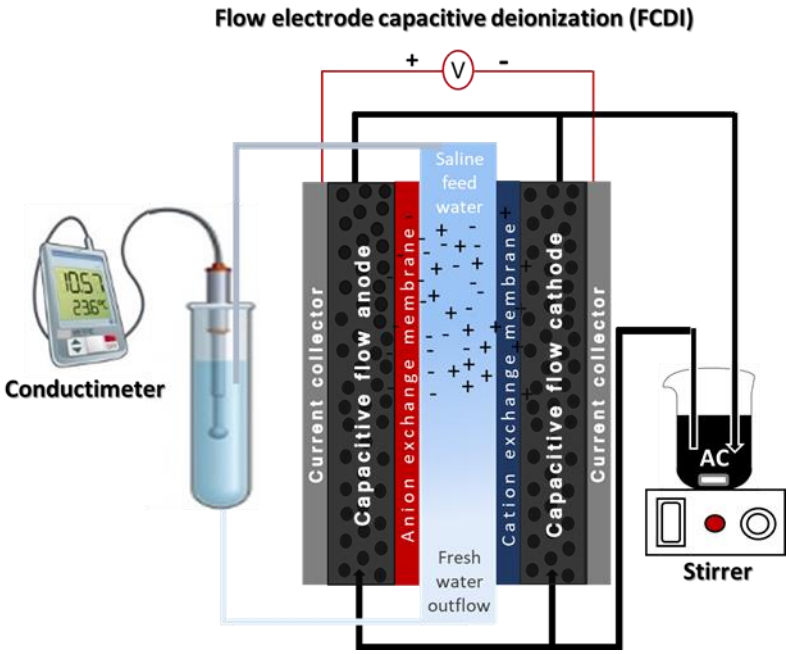

Fig. 1: Schematic diagram of FCDI set up

2.4. Physical Characterization

Scanning electron microscopy (SEM) was used to analyze the structure of the samples (SEM, Hitachi S4800, Tokyo, Japan). The structural properties were studied by using Raman spectroscopy (HORIBA Xplora, Minami-ku Kyoto, Japan) and X-ray diffraction (XRD diffractometer (Pan Analytical X'pert Phillips, Lelyweg, EA Almelo Netherlands) was used to investigate the crystallinity of the carbon. X-ray photon electron spectroscopy (XPS) (ESCALAB 250 Thermo Electron, Strasbourg, France) was done to investigate the atomic composition and chemical functional groups (chemical moieties) of the materials. For the XPS analysis, the excitation source was a monochromatic source Al Kα anode with photo energy that was observed at 1486.6 eV. The analyzed surface has a diameter of 500 μm. The photoelectron spectra were calibrated in terms of bond energy with respect to the energy of the C=C component of carbon C1s at 284.4 eV. Surface area was obtained using N_2 adsorption/desorption at 77 K. S_{BET} was the specific surface area calculated by the Brunauer-Emmett-Teller (BET) method (Micromeritics 2020 ASAP, Merignac France). Vt was the total pore volume calculated from the amount adsorbed at a relative pressure (P/P^0) of 0.99, V_{meso} was the mesopore volume calculated by the Barrett-Joyner-Halenda (BJH) model. Average particle size of the carbon was measured by Anton Paar (litesizer

500 France). Dynamic viscosity was measured using Anton Paar Rheometer Physica MCR 301(Anton Paar GmbH, Graz, Austria). Particle size distribution was also measured by Anton Paar Particle Lite Sizer (Anton Paar GmbH, Graz, Austria). The stability of the different activated carbon slurries in function of time was measured by Formulaction TURBISCAN.

2.5. FCDI measurement

The feed solution, saline water at 5 g/L (86.5mM, 70 mL) was made to pass through a spacer sandwiched in between cation and anion exchange membranes that are encased in a plastic plate placed in-between the current collector and the cell. The flow rate of the feed solution was maintained at a constant flow rate of 3 mL min^{-1}. The feed electrodes at 10 wt. %; containing 7.8 g of AC/FAC was dissolved in 70 mL of 1 g/L NaCl solution and stirred after sonication to form slurry electrodes were circulated in a closed cycle method in which both the anionic and cationic electrodes are being re-circulated in a reservoir; this allows co-mixing of charged ions outside the cell as shown in **Erreur ! Source du renvoi introuvable.** while **Fig. 2** shows the cell component used for this experiment. The flow rate of the electrode was operated at a constant flow rate of 40 mL min^{-1}. The initial conductivity of the feed solution and that of the effluent was monitored at room temperature by an ion conductivity meter (Hannah Instrument). Potentiostat operating at constant voltage of 1.0 V applied to the FCDI cell during the course of the experiments. The current from the FCDI unit cell was consequently measured during the experiment.

FCDI performance indicators of this experiment were calculated from the following parameters:

Desalination efficiency (DE, η) was calculated using equation (2):

$$\eta\ (\%) = \frac{(Co - Cf)}{Co}\ x\ 100 \quad (1)$$

Where η is the salt removal efficiency, C_0 and Cf are the initial and final concentrations ($mol.L^{-1}$)

Salt removal rate (SRR). This relates to the amount of salt adsorbed (mol) per FE-FS contact area (A in cm^2) per unit time (in s) and it is calculated by equation (3):

$$SRR = \frac{(Co - Cf)\ X\ V}{A\ X\ t} \quad (2)$$

Where V is the volume of the solution (L) and A is the contact area between FE: FS and t is the charging time.

Charge efficiency (CE) is the ratio of salt or moles of ions adsorbed to the quantity of charge passed into the system and was calculated by equation (4):

$$CE = \frac{z\,(Co - Cf)\,V\,F}{\int I dt} \quad (3)$$

Where z is the equivalent charge of the ions, F is the Faradaic constant and $\int I dt$ is the integrated quantity of charge passed to the system as a function of time.

Reynolds number which shows the flow nature of the electrode (collision pattern) in the flow channel was calculated using equation (4):

$$Re = \frac{\rho\, v\, D}{\eta} \quad (4)$$

Where ρ is the density of flow-electrode, v is the velocity of flow-electrode in the flow channel calculated from flow rate of the flow electrode (0.0024 $m^3\ h^{-1}$) to the area of the flow cell (5.4 x 10^{-6} m^2), D is the hydraulic diameter of the flow channel, 2.6 mm; η is the average coefficient of dynamic viscosity of flow-electrode as a function of shear rate at 25 °C.

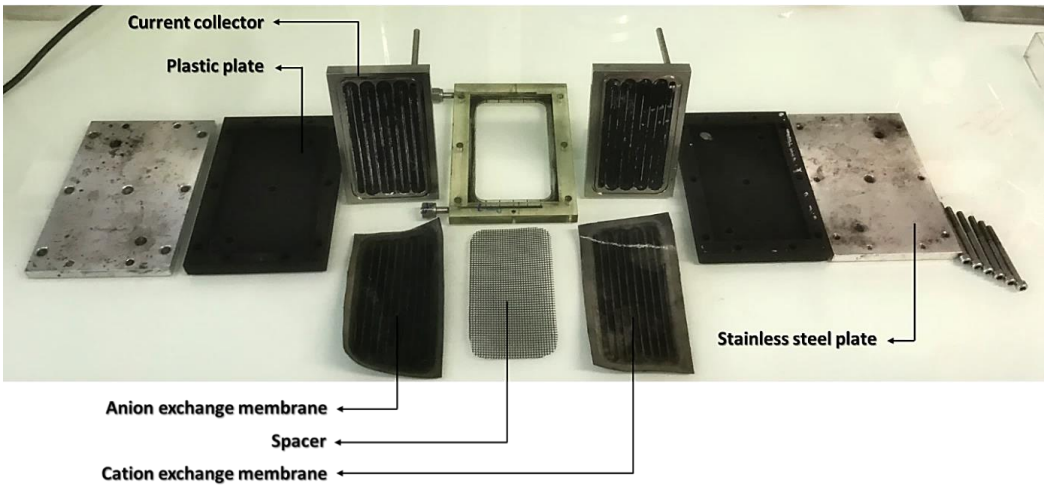

Fig. 2: Individual cell component of FCDI

3. Results and discussion

3.1. Morphology properties of PAC and FAC

The morphology of AC and FAC was examined by scanning electron microscope (SEM). As shown below in

Fig. 3 (a-d), the commercial AC is of no definite shape with presence of rough surfaces. As observed from SEM, FAC showed smoother surfaces for the particles.

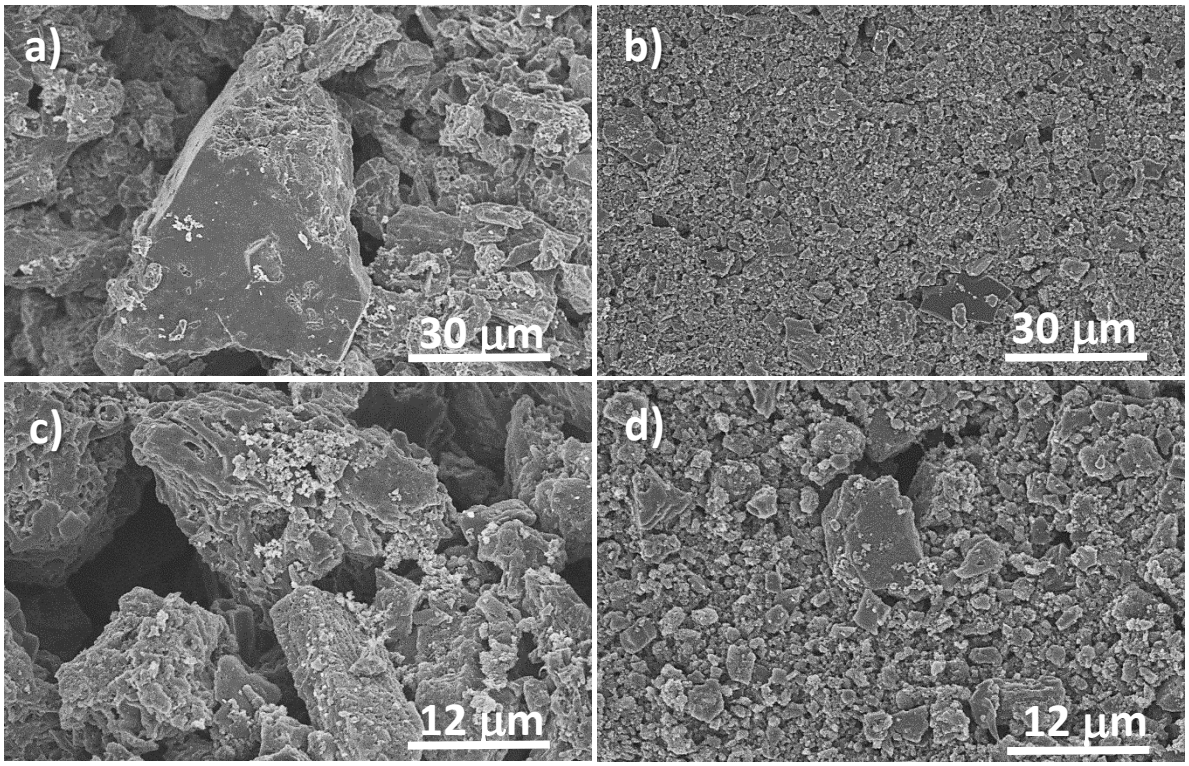

Fig. 3: Scanning electron microscope (SEM) top view images of (a), (c) normal or pristine AC and (b), (d) FAC after 90 min of grinding.

As the shape of the particles was determined by SEM, the particle size of AC and FAC was investigated by dynamic light scattering (DLS) at constant volume ratio to reveal the trend in particle size as grinding time increases. As shown in **Fig. *4***, the result of DLS corroborates that of SEM in which pristine AC has largest particle size. Also, the hydrodynamic diameter of AC was recorded to be 2.63 µm whereas it was 2.47, 2.32 and 2.12 µm for FAC ground at 30, 60 and 90 min. respectively.

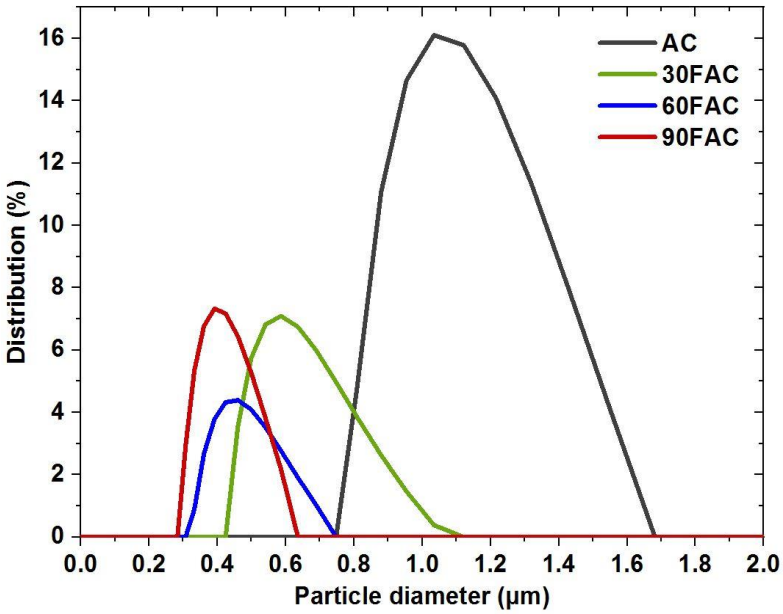

Fig. 4: Particle size of AC and FAC at 30, 60 and 90 min ball milling respectively.

3.2 Structural properties

The structural properties of the samples were investigated by Raman and X-ray diffraction spectroscopy. Raman spectroscopy analysis was done to investigate the effect of grinding on the structure of the carbon lattice. All of our carbon materials have characteristics features at 1350 cm^{-1} and 1590 - 1610 cm^{-1} corresponding to D and G bands of graphitic carbon respectively. D band arises from a defect that is based on out of plane vibration in carbon structure while G band relates to the ordered structure of graphite crystals [18]. No Raman shift was observed in all cases as made evident in **Fig. 5** (a). Also, based on the values of intensity ratio (R) which is used to observe the level of disorder in carbonaceous materials, FAC showed no significant difference in defect on comparison with normal AC (FAC, R = 1.2; normal AC, R = 1.0). This shows that grinding does not affect the structural arrangement in our carbon lattice.

XRD patterns of normal AC and FAC at all conditions do not show any significant change or shift in the interlayer spacing (i.e., the distance between the adjacent sheets or layers of the carbon arrangement remain the same; indicating that the integrity of the normal AC was preserved) as shown in **Fig. 5** (b). They all demonstrated prominent diffraction peaks of graphitic carbon at 2 Θ = 26 ° and 44 ° corresponding to 002 and 100 or 101 planes of graphite respectively. The sharp diffraction peaks at 002 indicates the presence of graphite microcrystalline structure [19].

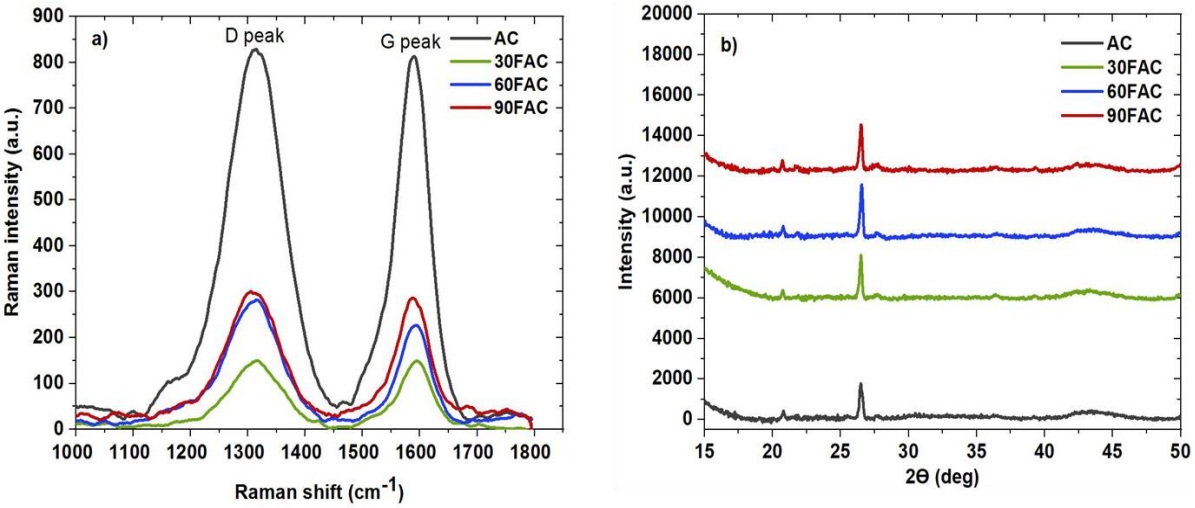

Fig. 5: (a) Raman spectra and (b) XRD of AC and FAC at 30, 60 and 90 min grinding respectively.

Also, chemical moieties and composition of AC and FAC were investigated by FTIR and XPS. **Fig. 6** (a) shows the FTIR spectra of both normal AC and FAC. The peak at 2925 cm^{-1} is associated with CH_3 stretching [20] and the peak at 1490 cm^{-1} is due to the stretching vibration of benzene ring [21]. The peak at 2200 cm^{-1} is due to N-N stretching [22]. The peak at 1450 cm^{-1} is due to C–H stretching while the peak at 1022 cm^{-1} is associated with C–O bond from esters and ethers [23]. In all cases, there seem to be no obvious significant peak reduction in the functional groups of all the samples. This shows that the surface chemistry was preserved and grinding has no effect on it.

Also, further probe by XPS showed no band reduction of the functional groups in FAC in comparison to normal AC. Furthermore, and according to XPS analysis, the atomic percentage of both FAC and PAC for C1s and O1s is the same (C1s = 94.80 %, O1s = 5.20 %). **Fig. 6** (b) shows the whole spectra of the samples while (c) and (d) shows the resolved C 1s spectrum of PAC and FAC into their individual peaks respectively. Binding energies of 284.5, 285.8, 287 and 288 eV present in the distribution of the peaks corresponded to C=C, C-O, C=O and -COO- respectively [24].

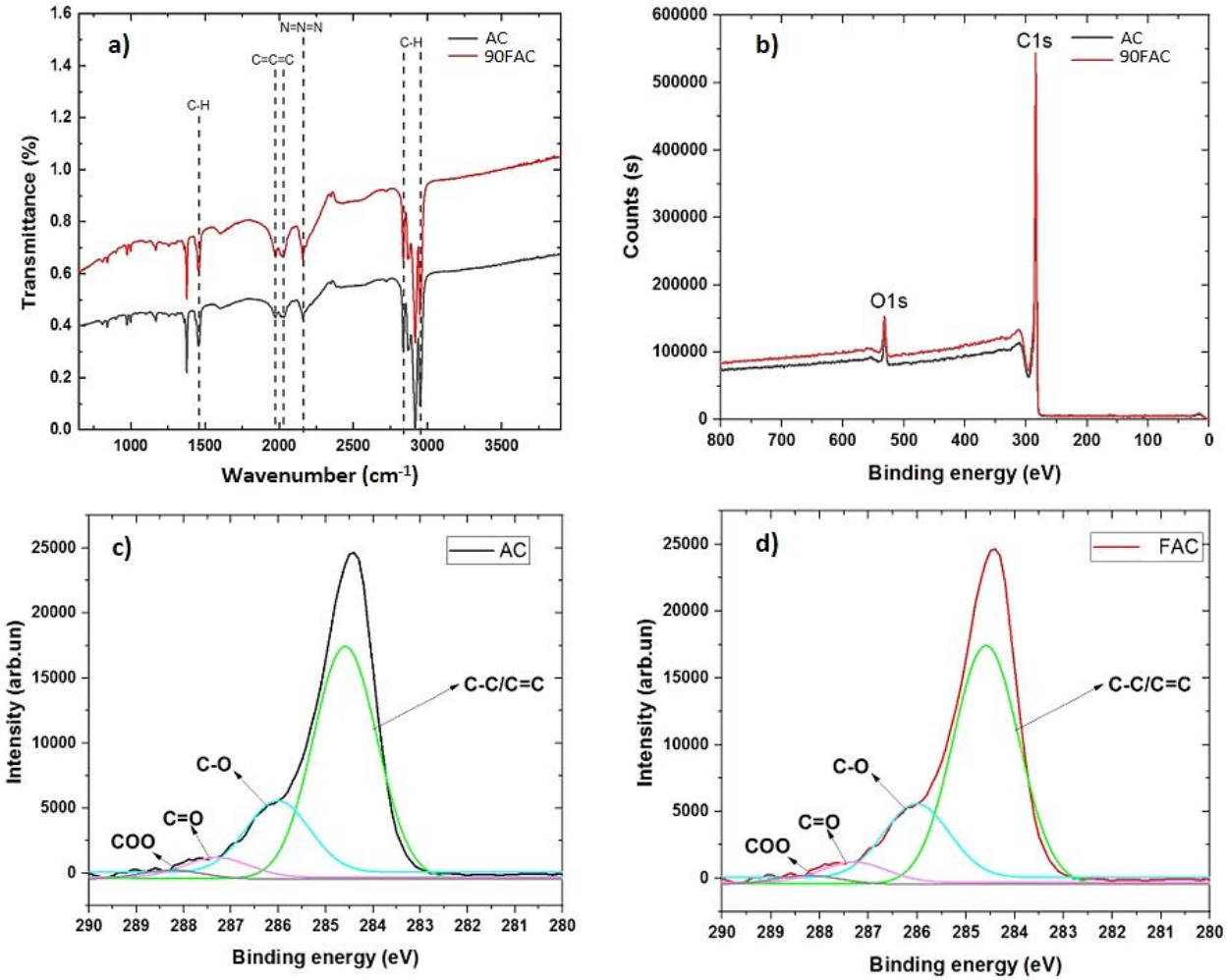

Fig. 6: FT-IR spectra of (a) normal or pristine AC and FAC, (b) XPS whole survey of pristine AC and FAC (c) and (d) Deconvoluted XPS spectra of C1s of pristine AC and FAC respectively.

3.3. Textural Properties

The textural properties of AC and FAC were verified and compared as presented in **Table 2**. No significant difference in effect of grinding was observed on the specific surface area of 30 and 60 min FAC but at 90 min FAC, an increase in the specific surface of the material was observed. This could be due to the fact that greater percentage of the particles are found at the surface of the material thus enabling particles of larger ratio of surface to volume. Also, there could be generation of higher porosity at this grinding time. Adsorption isotherm for our carbon material, between 0 and 0.1 relative pressure was calculated using t-plot method. From **Fig. 7** (a), the isotherm curve of normal AC is a type I isotherm based on IUPAC classification indicating the presence of micropores [25].

Pore size distribution which indicates the range of pores accessibility for a molecule or ions was used as shown in **Fig. 7** (b) to verify the region of ions adsorption in our carbon materials. Using Micropore analysis (M-P) method and as indicated in **Fig. 7** (b), the pore size distribution of AC shows dominant adsorption characteristic at the micropore region (< 2 nm) with an average pore size value of 0.3 nm.

Table 2. Textural parameters of AC and FAC at different grinding times

Sample	V_t ($cm^3 \cdot g^{-1}$)	S_{BET} ($m^2 \cdot g^{-1}$)
Normal AC	0.67	839.27
30min FAC	0.68	826.22
60min FAC	0.66	817.30
90min FAC	0.68	850.05

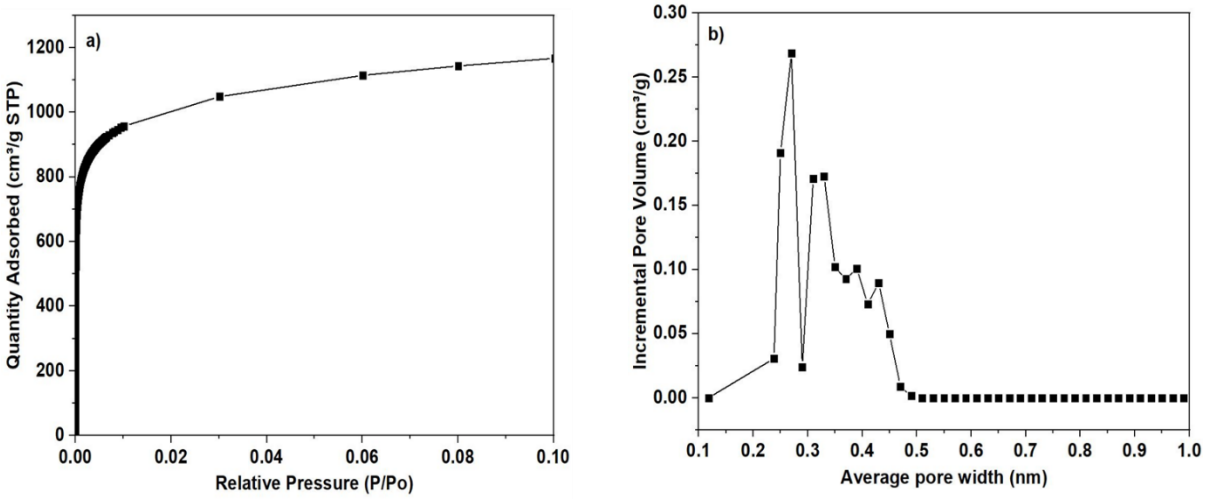

Fig. 7: Nitrogen adsorption-desorption isotherm of AC (**a**) and pore width distribution (b) of normal AC

3.4. Rheology and zeta potential studies

Here we investigate the correlation between particle size, zeta potential and dynamic viscosity of the slurry. The dynamic viscosity of the slurry electrode was measured as a function of shear rate. Dynamic viscosity is the term used to describe resistance to flow of liquid while shear rate describes the speed of deformation of the slurry under applied force. The dynamic viscosity was determined at a constant concentration of 10 wt. % carbon content in the slurry. From **Fig.** *8* (a), it is obvious that the slurry follows the comportment of a non-Newtonian fluid (Shear Thinning effect) in which the viscosity of the slurry decreases with increasing shear rate [26]. Also, it can be concluded from **Fig.** *8* (a) that viscosity of FAC increases with increasing grinding time although no significant difference was observed between 30 min and 90 min of grinding. Reduction in particle size is associated with higher particle numbers thus with small particles, there tend to be increase in the number of particle interactions and consequently an increase in resistance to flow; a dominating factor at low shear rate [27]. Also, reducing particle size has a significant positive impact on surface area of area between liquid and solid phases;

resulting in additional energy dissipation due to friction hence increasing viscosity. This effect becomes less significant as shear rate increases; intra-particle interactions become relatively less effective. As for normal AC, its viscosity could be as a result of high aggregation due to its large particle size. Also, viscosity decreases with increasing particle size distribution (PSD) [28] and as shown in **Fig. *4***, normal AC exhibited the highest particle size distribution; this could account for its relatively lower viscosity as grinding effect becomes more prominent. Particles possessing large distribution (high poly-dispersity) have high tendency to aggregate (pack) easily over the narrowly dispersed ones. This shows that suspension or dispersion with high poly-dispersed particles have free space for individual particle to move around with ease and as such, flow easily thus implying lower viscosity [28].

Zeta potential measurement is related to the charges of particles in dispersion or suspension. This factor is also associated with electrostatic repulsive forces between particles under the influence of electric field. An increase in this repulsive force (increase in zeta potential) prevents particles aggregation. Dispersion with high magnitude of zeta potential will induce a weak electrostatic attraction between particles and consequently a high viscosity of the slurry. Slurries prepared with low size particles are expected to have these characteristics as they are loosely bound (inter-particle interaction reduces as repulsive force increases; leading to increase in zeta potential). Normal AC shows the lowest potential due to aggregation as a result of large particle size; a result that is expected as shown in **Fig. *8*** (b). For FAC, as particle size decreases, the dispersion slurries of these materials tend to be more stable due to increasing loosening of the particles thus there is high tendency of resistance to flow of particles and consequently yielding high zeta potential.

In general, and from our experimental results, we can conclude that zeta potential increases with decrease in particle size and consequently, dispersion with lower particle size tend to be more stable as they are loosely bound thus leading to increase in viscosity [29, 30]. Our result correlates with what is reported in literature [29-32].

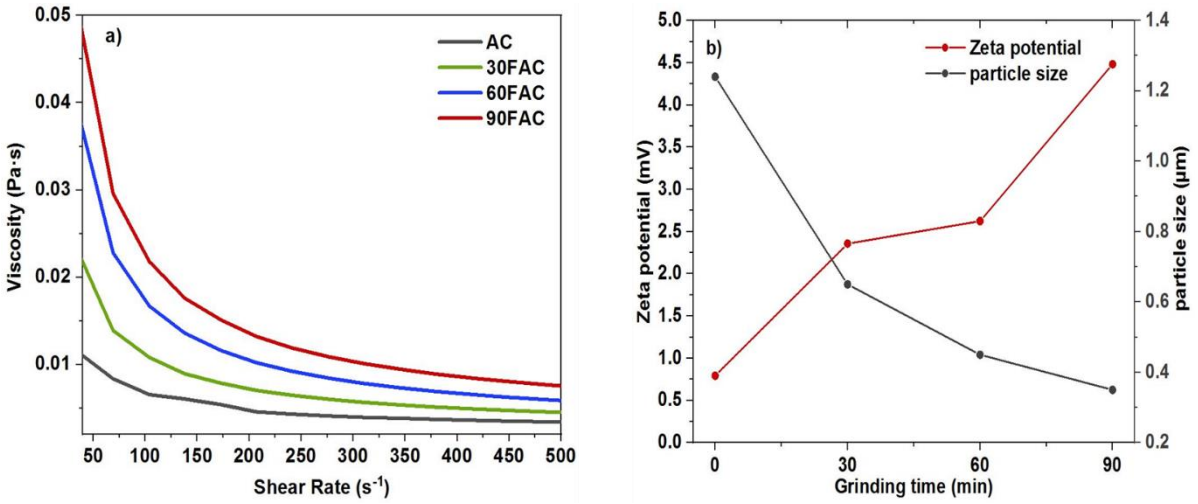

Fig. 8: (a) Rheological properties (b) Zeta potential, of AC and FAC suspensions in 1g/L NaCl electrolytes solution

3.5. Reynolds number

The Reynolds number was calculated using equation (5) for the different slurry electrodes and the results are given in **Table *3***. From the table, Reynolds number of the slurries decreases with increasing viscosity. Reynolds number relates to the level of flow pattern (turbulence or laminar) in fluid system. The calculated Reynolds number in all our carbon slurries as presented in **Table *3*** shows that the prevalent flow pattern in our channel is laminar in nature thus implying that the carbon particles in the slurry flow along with the electrolyte solution in the flow channel of electrode compartments. A similar study was also reported by Peng *et al.* [33]. For a laminar flow, the Reynolds number is usually below 2,300 and when it is within the range of 2,300 and 4000; the pattern of flow is said to be turbulent regardless of the nature of the fluid [34].

Table 3: Reynold's number of different feed electrode composition

Material	**Reynolds n°**
AC	58.21
30FAC	38.57
60FAC	26.57
90FAC	20.53

3.6. Physical stability

The physical stability or sedimentation rate of the different activated carbon dispersions in function of time was investigated using multiple light scattering technology, turbiscan. The destabilization kinetics of activated carbon suspensions at 10 % wt. volume ratio along 30 min (experimental time) was detected as grinding time increase. Turbiscan stability index (TSI) scale shown in Fig. 9 enables to quantify the stability, with values established based on the correlation with visual methods. Below level A on the TSI visual scale, no destabilization is observed, level A marks the beginning of a very early stage destabilization, level B indicates the beginning of destabilization, level C and D refer to a large sedimentation stage. As shown in Fig. 9, pristine AC dispersion begins to destabilize after 2 minutes and enters the large sedimentation phase (C) in less than 5 minutes. On the other hand, no sedimentation was observed for 60FAC and 90FAC suspensions all along the 30 minutes. It can be concluded from Fig. 9 that the physical stability of AC suspensions increase with the increase of grinding time, although no difference was observed between 60 min and 90 min of grinding. Particle size reduction leads to slower sedimentation rate. In the case of FAC, particles will stay suspended and well dispersed in the solution for a longer time, which increases the intra-particle interactions in solution. Interestingly, these results perfectly correlate with rheology and zeta potential results, explaining the behavior of different particle size AC suspensions as flow electrodes.

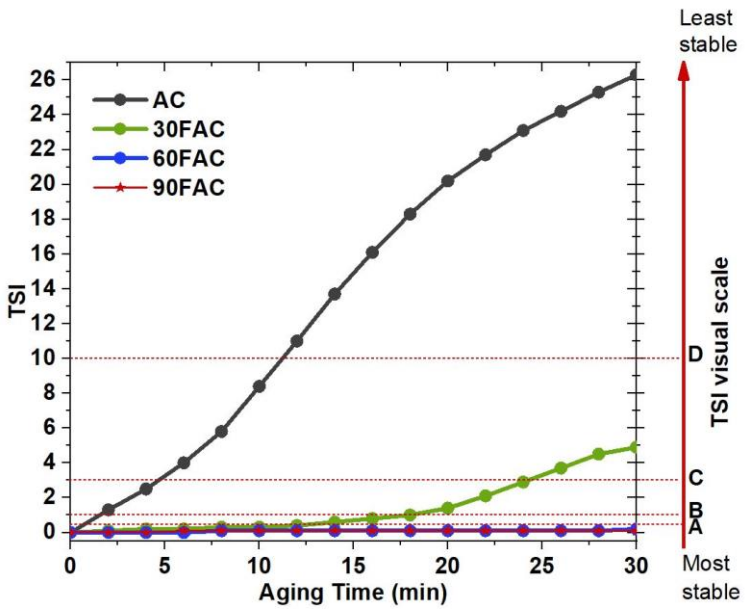

Fig. 9: Turbiscan stability index (TSI) of AC and FAC suspensions in 1g/L NaCl electrolytes solution

3.7. Desalination

The electro-sorption behavior of FAC at different time interval was verified and compared with normal AC. In all cases, FAC flows as much as normal AC without clogging at 10 wt. % of operation. FAC offers tremendous improvement with respect to salt adsorption on comparison with normal AC due to improved area of contact within the carbon network. Furthermore, FAC ground at 90 min competes excellently well and possessed the highest desalination rate over all its counterpart and normal AC as shown in Fig. 10 (a).

FCDI performance indicators (equation 1-3) such as DE and SRR (Fig. 10 b), SRR is calculated from Fig. 10 (a) and CE (Fig. 10 c) is calculated from Fig. 10 (a) and desalination integrated current response show that in all cases, FAC (30, 60 and 90 min) exhibited higher performance over normal AC. More so, 90 min FAC exhibited the highest performance among its counterpart possibly due to its improved and sufficient ions diffusion pathways (easy ion diffusion from the membrane to the pores of fine particles of flow electrode); this fact is made evident by the sharpest drop in ionic conductivity or initial concentration of 90 min FAC in Fig. 10 (a). Lower desalination performance of 30 and 60 min FAC could be as a result of their lower force of repulsion making the particle not easily accessible thus causing long ion diffusion pathway (between membrane and carbon slurry) to the carbon pores of the flow electrodes. This consequently leads to lower performance metrics of these flow electrodes.

For further investigation into reaching a compromise in grinding time, we ball milled the normal AC for 5 h and verified its propensity for desalination. Surprisingly, no significant difference was obtained in the desalination performance between 90 min and 5 h FAC (≤ 5 % improvement) as shown in Fig S1 (a-d) in the supplementary information. This proves 90 min of ball milling (grinding) is sufficiently efficient for our experiment. Our strategy involves a very simple physical method of maximizing commercially made activated carbon particle size and through this method, a tremendous improvement in desalination was observed. With our strategy, we believe that ions in the saline solution can diffuse faster into the pores of the flow electrode due to greater area of contact created as a result of low particle size thus allowing better area of contact within the carbon network. Also, we compared our results to performance of some flow-electrode capacitive deionization (FCDI) cells recently reported in literature as presented in **Table 4**. From the table, it is apparent that FAC offers tremendous improvement in performance matrices over some AC that are modified with expensive additives unlike the simple modification method reported in this paper thus asserting the propensity of FAC as a potential flow electrode.

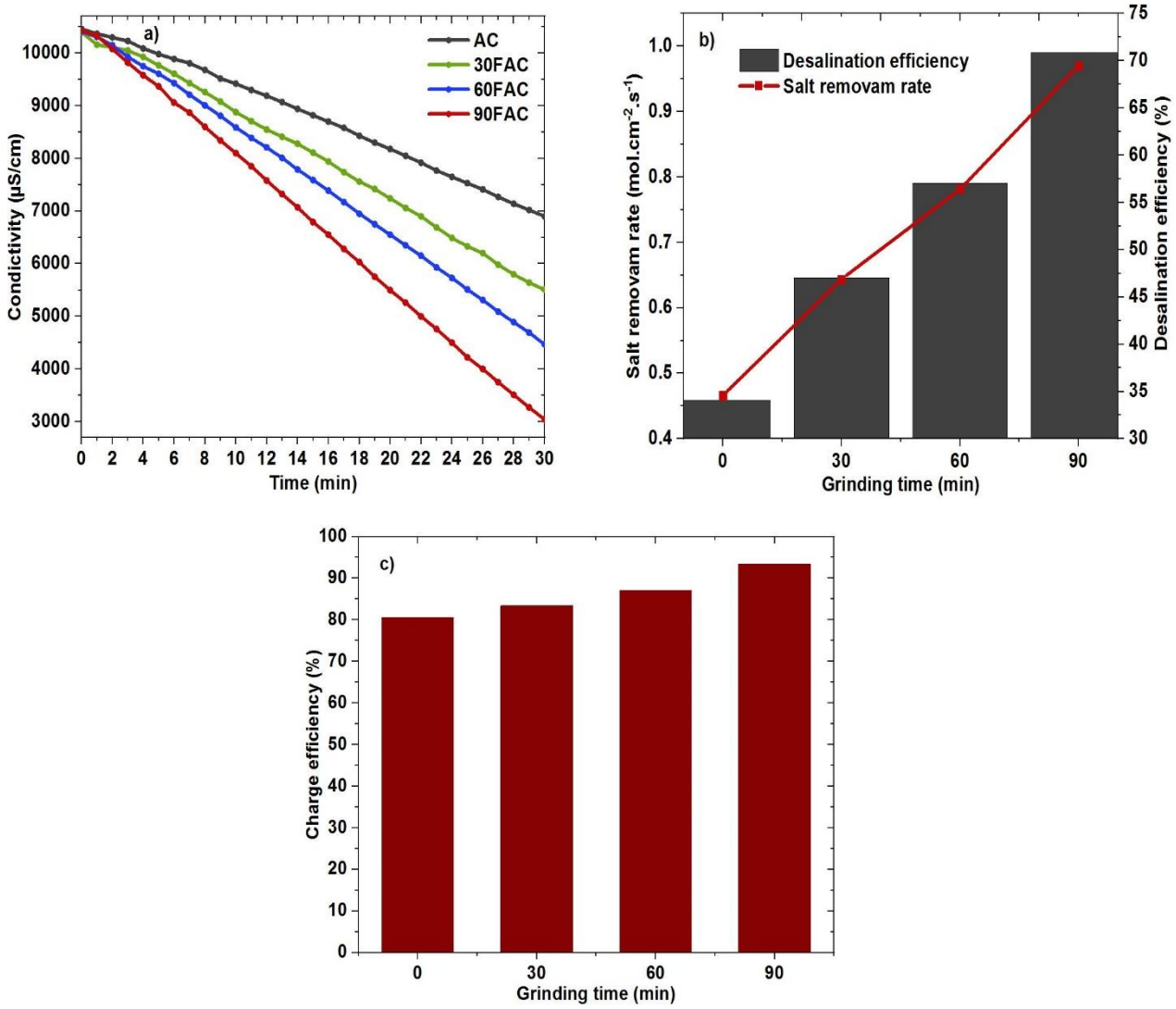

Fig. 10: Desalination conductivity curve (a) AC and FAC at different time (b) Salt removal rate and desalination efficiency and (c) charge efficiency of normal AC and FAC at different time interval respectively.

To mention that activated carbon is a very stable material as flow electrode in FCDI, the same electrode can be used for many consecutive adsorption/desorption cycles with conserved performance. However, in case of deterioration of AC material inside the electrode, it can be replaced to regenerate the whole system.

Another stability related risk in FCDI system is clogging problems in the ion exchange membranes. These membranes can be washed (chemical washing) or simply replaced in case of non-reversibility.

Table 4: Recent advances in FCDI cell performance.

Electrode material	Electrolyte	Voltage (V)	Carbon Loading (wt. %)	FS [NaCl] ($g\ L^{-1}$)	DE (%)	SRR (mg/min . cm^2)	CE (%)	Ref
AC	H_2O	1.2	5	35	68	0.34	-	1
AC	H_2O	-	23	5	18	-	-	4
Spherical AC	NaCl+H_2O	1.2	6.98	35	19	-	-	8
AC DARCO	H2Q/Q	1.2	1	2		0.42 μg/min.cm^2	-	11
AC+CB	Na2SO4+ H_2O	4.8	20	0.65	-	0.208	69.50	34
Spherical AC+CNT	NaCl+H_2O	1.6	7.41	11.70	-	8.32 mg/s m^{-2}	93.30	35
AC Norrit	H_2O	1.2	5	5.85	80	-	100	36
AC Darco +CB	H_2O	1.2	10	2	-	0.707 μg/s.cm^2	98	37
AC MSC-30	NaCl+H_2O	1.2	5	35	62.90	-	89.70	38
AC BEADS Modified with VBTAC and S4VBS	NaCl+H_2O	1.2	35	5	27.20	5.5 mm/ $s.m^2$	85.60	39
AC DARCO	H_2O	2.0	10	2	-	0.14μg/ $cm^2\ s^{-1}$	95	40
AC NORRIT	H_2O	1.2	5	1	99	-	97.9	41
FAC DARCO	NaCl+H_2O	1.0	10	5	70.85	0.970	93.41	T W

VBTAC: Vinyl benzyl trimethyl ammonium chloride; S4VBS: sodium 4-vinylbenzenesulfonate,MSC Maxsorb Carbon ; T W: This work

5. Conclusion and perspective

In summary, flow electrodes were made by simple grinding of powdered AC at different time interval (30, 60 and 90 min) and tested in comparison with pristine AC for desalination application by FCDI process. In all conditions, all the fine AC (FAC) flow just as much as pristine AC at 10 wt. % without clogging in the FCDI cell. On the basis of our findings (experimental analyses), particle size reduction has direct effect on viscosity but the textural, structural properties and chemical moieties of FAC remain unchanged in comparison with pristine AC. Interestingly, the desalting performance of FAC outperforms that of pristine AC due to improved contact area within carbon network caused as a result of reduction in particle size and easy pores accessibility. In addition, we verified that 90 min of ball milling is enough to optimize the performance of AC as flow electrode at moderate weight percent of carbon loading. It is no doubt that improvement in material aspect of FCDI is an important backbone that is necessary towards optimization of this second generation water desalination technology. However, improvement of this aspect is mutually exclusive as one parameter could be affected while improving a certain challenge. To offset this compromise requires intensive research through ways such as molecular dynamic simulation or computational software (for theoretical observation) that can improve experimental procedures should be encouraged. Though fine AC offers tremendous improvement in desalination nevertheless, its high viscosity is a setback (low carbon feed into the cell) thus further research should be conducted on viscosity reduction of this carbon.

Author Contributions: Conceptualization: G.F and M.B.; Methodology: M.B and M.C.; Formal analysis: Physico-chemical analysis by G.F, and M.B. Investigation: G.F and M.T.; Resources: F.Z., M.B., P.S. and M.C.; Data curation: G.F and M.T.; Original draft preparation: G.F.; Writing, review and editing: G.F., F.Z., M.B. and M.C.; Visualization: F.Z., M.T., M.B. and M.C.; Supervision: F.Z., M.B., P.S. and M.C.; Project administration: M.B., F.Z., P.S. and M.C. All authors have read and agreed to the published version of the manuscript.

Funding: The authors gratefully thank "Axe Water" and "Axe Energy" in European Institute of Membranes (IEM) for the funding received and the Federal Government of Nigeria through Tertiary Education Trust fund (TETFUND) and Campus France (CF) for the Ph.D. funding of Gbenro Folaranmi with the funding number CAMPUS FRANCE 914886H.

Acknowledgments: Special thanks to all the contributing authors, Institute European des Membranes (IEM), Fida Thanos for the planetary ball mill operation and Gatien Roland for the preliminary studies on the FCDI cell.

Conflicts of Interest: The authors declare no conflict of interest.

References

1. Jeon, S.-i.; Park, H.-r.; Yeo, J.-g.; Yang, S.; Cho, C. H.; Han, M. H.; Kim, D. K. Desalination via a new membrane capacitive deionization process utilizing flow-electrodes. *Energy Environ. Sci*. **2013**, 6, 1471−1475
2. Folaranmi G, Bechelany M, Sistat P, Cretin M, Zaviska F. Towards electrochemical water desalination techniques: A review on Capacitive Deionization, Membrane Capacitive Deionization and Flow Capacitive Deionization. *Membranes* **2020**, 10**,** 96.
3. Campos J.W., Beidaghi M., Hatzell K.B., Dennison C.R., Musci B., Presser V., Kumbur E.C., Gogotsi Y. Investigation of carbon materials for use as a flowable electrode in electrochemical flow capacitors. *Electrochim. Acta* **2013,** 98 123–130.
4. Hatzell, K. B.; Hatzell, M. C.; Cook, K. M.; Boota, M.; Housel, G. M.; McBride, A.; Kumbur, E. C.; Gogotsi, Y. Effect of oxidation of carbon material on suspension electrodes for flow electrode capacitive deionization. *Environ. Sci. Technol*. **2015,** 49, 3040−3047.
5. Aworn A, Thiravetyan P, Nakbanpote W. Preparation of CO_2 activated carbon from corncob for monoethylene glycol adsorption, *Colloids Surf. A* **2009, 333,** 19–25
6. Konwar, Y. Sugano, R.S. Chutia, A. Shchukarev, P. Mäki-Arvela, R. Kataki, J.-P. Mikkola, Sustainable synthesis of N and P co-doped porous amorphous carbon using oil seed processing wastes, *Mater. Lett.* **2016,** 173, 145–148.
7. Boota, M.; Hatzell, K. B.; Beidaghi, M.; Dennison, C. R.; Kumbur, E. C.; Gogotsi, Y. Activated carbon spheres as a flowable electrode in electrochemical flow capacitors. *J. Electrochem. Soc*. **2014,** 161, 1078−1083.
8. Yang S., Choi J., Yeo J., Jeon S., Park H., Kim D.K.K Flow-electrode capacitive deionization using an aqueous electrolyte with a high salt concentration. *Environ. Sci. Technol*. **2016**, 50, 5892–5899
9. Xu X, Wang M, Liu Y, Lu T and Pan L. Ultrahigh Desalinization Performance of Asymmetric Flow-Electrode Capacitive Deionization Device with an Improved Operation Voltage of 1.8 V. *ACS Sustainable Chem. Eng.*, **2017,** 5**,** 189 −195
10. Doornbusch G. J., Dykstra J. E., Biesheuvel P. M. and Suss M. E. Fluidized bed electrodes with high carbon loading for water desalination by capacitive deionization, *J. Mater. Chem. A*, **2016,** 4, 3642 −3647
11. Ma J, He D, Tang W, Kowalski P, He C, Zhang C and Waite T. D. Development of Redox-Active Flow Electrodes for High-Performance Capacitive Deionization, *Environ. Sci. Technol.*, **2016,** 50**,** 13495 −13501
12. Aranzazu C.O, Robert A.W.D. Understanding the performance of flow-electrodes for capacitive deionization through hydrodynamic voltammetry. *Che Engr J.* **2021,** 406, 126826
13. Kuo F, Hui G, Wenyan H, Fei P and Kaijun W. Revealing the intrinsic differences between static and flow electrode capacitive deionization by introducing semi-flow electrodes. *Environ. Sci Water Res. Technol.*, **2020**,6, 362-372
14. Partlan, E., Davis, K., Ren, Y., Apul, O.G., Mefford, O.T., Karanfil, T., Ladner, D.A. Effect of bead milling on chemical and physical characteristics of activated carbons pulverized to fine sizes. *Water Res.* **2016,** 89, 161–170.
15. Matsui, Y., T. Aizawa, F. Kanda, N. Nigorikawa, S. Mima, and Y. Kawase. Adsorptive removal of geosmin by ceramic membrane filtration with superpowdered activated carbon. Journal of Water Supply: Research and Technology, AQUA, **2007**. 56, 411-418.
16. Ando N, Matsui Y, Kurotobi R, Nakano Y, Matsushita T and Ohbno K. Comparison of natural organic matter adsorption capacities of super-powdered activated carbon and powdered activated Carbon. *Water Research*, **2010**. 44, 4127-4136

17. Chen D, Feng H, Li J. Graphene oxide: preparation, functionalization, and electrochemical applications. *Chem Rev*. **2012**; 11, 6027–53.
18. Shijie L, Kuihua H, Pengchao S, Jinxiao L, Chunmei L. High–performance Activated Carbons Prepared by KOH Activation of Gulfweed for Supercapacitors. *Int. J. Electrochem. Sci.* **2018,** 13, 1728 – 1743
19. Ng E.P, Mintova S. Quantitative moisture measurements in lubricating oils by FTIR spectroscopy combined with solvent extraction approach. *Micro chem. J*. **2011**. 98, 177–185.
20. Zhigang X, Wei G, Fangying J, Zhongrong S, and Yanling Zhao. Production of Biologically Activated Carbon from Orange Peel and Landfill Leachate Subsequent Treatment Technology. *Journal of chemistry*, **2014**, 10-18
21. Ying L, Xiaohui L, Wenping D, Lingli Z, Qiang K and Weiliang W. Efficient Adsorption of Sulfamethazine onto Modified Activated Carbon: A Plausible Adsorption Mechanism. *Scientific report.* **2017**, 7, 12437
22. Feng W, He P, Ding S. Oxygen-doped activated carbons derived from three kinds of biomass: preparation, characterization and performance as electrode materials for supercapacitors. *Rsc Adv.* **2016**. 6, 5949–5956
23. Ling Z, Ling-yu T, Yan L, Qi C. Coconut-based activated carbon fibers for efficient adsorption of various organic dyes. *RSC Advances* **2018**, 8,42280-42291
24. Thommes M.; Kaneko K.; Neimark A. V.; Olivier J. P.; Rodriguez-Reinoso, F.; Rouquerol, J.; Sing, K. S. W. Physisorption of gases, with special reference to the evaluation of surface area and pore size distribution (IUPAC Technical Report). *Pure Appl. Chem.* **2015**, 87, 1051−1069.
25. Amidon G.E., Bergren M.S., Grant D.J.W., Marshall K., Itai S., Physical test methods for powder flow characterization of pharmaceutical materials: a review of methods stimuli to the revision process, *Pharmacopeial Forum,* **1999**, 25, 8298–8308
26. Hou H., Sun C.C., Quantifying effects of particulate properties on powder flow properties using a ring shear tester, *J. Pharm.Sci*. **2008,** 97, 4030–4039.
27. Qi Z, Brian A, Ian L, Peter J. S, David A.V. M. Effect of host particle size on the modification of powder flow behavior for lactose monohydrate following dry coating. *Dairy Sci. Technol*. **2010,** 90, 237–251
28. Sven K, Antoinette Y.V, Lukas A, Thorsten T, Rainer T. Zeta potential and long-term stability correlation of carbon-based suspensions for material jetting**.** *Open Ceramics*. **2020**, 4, 100037
29. Peng L, Xueliang S, Yanhong B, Helan Z, Xufei Y, Yong J, Panpan L, Xia H. Optimized desalination performance of high voltage flow-electrode capacitive deionization by adding carbon black in flow-electrode. *Desalination*, **2017**, 420, 63-69
30. Reynolds O. An Experimental Investigation of the Circumstances Which Determine Whether the Motion of Water Shall Be Direct or Sinuous, and the Law of Resistance in Parallel Channels, Philosophical Transactions of the Royal Society of London. **1883**, 174, 935-982
31. Kexin T, Sotira Y, Yuping L and Costas T. Enhanced Water Desalination by Increasing the Electroconductivity of Carbon Powders for High-Performance Flow-Electrode Capacitive Deionization *Sustainable Chem. Eng*. **2019**, 7, 1085−1094
32. Daniel M and Marta C. H. Influence of Feed-Electrode Concentration Differences in Flow Electrode Systems for Capacitive Deionization. *Ind. Eng. Chem. Res*. **2018,** 57, 8802−8809
33. Calvin H, Jinxing M, Changyong Z, Jingke S and David W.T. Short-Circuited Closed-Cycle Operation of Flow-Electrode CDI for Brackish Water Softening. *Environ. Sci. Technol*. **2018,** 52, 9350−9360
34. SeungCheol Y, Sung-il J, Hanki K, Jiyeon C, Jeong-gu Y, Hong-ran P and Dong K.K. Stack Design and Operation for Scaling Up the Capacity of Flow-Electrode Capacitive Deionization Technology. Sustainable Chem. Eng. **2016**, 4, 4174−4180
35. Hong-ran Park, Jiyeon C, Seungcheol Y, Sung J.K, Sung-il J, Moon H.H and Dong K K. Surface-modified spherical activated carbon for high carbon loading and its desalting performance in flow-electrode capacitive deionization. *RSC Adv*., **2016**, 6, 69720
36. Ma J, C. He, He D, Zhang C. and Waite T. D. Analysis of capacitive and electrodialytic contributions to water desalination by flow-electrode CDI, *Water Res.*, **2018,** 144**,** 296 —303
37. Gendel Y, Rommerskirchen A.K.E, David O and Wessling M. Batch mode and continuous desalination of water using flowing carbon deionization (FCDI) technology. *Electrochem. Commun*, **2014,** 46, 152-156
38. Yang, Y. He, L. Rosentsvit, Suss M.E., Zhang X., Gao T, Liang P, Flow-electrode capacitive deionization: a review and new perspectives, Water Res 200 (2021) 117222.

39. Ashrafizadeh S N, Ganjizade, A. Navapour A. A brief review on the recent achievements in flow-electrode capacitive deionization, Korean Journal of Chemical Engineering 38(1) (2021) 1-7.